Genome-wide off-rates reveal how DNA binding dynamics shape transcription factor function

Wim J. de Jonge, Mariël Brok, Philip Lijnzaad, Patrick Kemmeren & Frank C.P. Holstege

Princess Máxima Center for Pediatric Oncology, Heidelberglaan 25, 3584 CS Utrecht, the Netherlands

Abstract

Protein-DNA interactions are dynamic and these dynamics are an important aspect of chromatin-associated processes such as transcription or replication. Due to a lack of methods to study on- and off-rates across entire genomes, protein-DNA interaction dynamics have not been studied extensively. Here we determine *in vivo* off-rates for the *Saccharomyces cerevisiae* chromatin organising factor Abf1, at 191 sites simultaneously across the yeast genome. Average Abf1 residence times span a wide-range, varying between 4.5 and 37 minutes. Sites with different off-rates are associated with different functional characteristics. This includes their transcriptional dependency on Abf1, nucleosome positioning and the size of the nucleosome-free region, as well as the ability to roadblock RNA polymerase II for termination. The results show how off-rates contribute to transcription factor function and that DIVORSEQ (Determining *In Vivo* Off-Rates by SEQuencing) is a meaningful way of investigating protein-DNA binding dynamics genome-wide.

Introduction

Processes that act on chromatin, such as transcription or replication, are controlled by molecular interactions. This includes proteins interacting with DNA. Protein-DNA interactions are dynamic and these dynamics are likely important to achieve appropriate regulation of DNA-dependent processes. During transcription for example, different types of transcription factors (TFs) are continuously interacting with chromatin in a variety of ways. Each brings different functions into play: opening or closing chromatin, creating loops, modifying or evicting nucleosomes, recruiting cofactors and, in the case of activation, ultimately causing formation of a pre-initiation complex that includes RNA polymerase (Hahn & Young, 2011; de Laat & Dekker, 2012; Spitz & Furlong, 2012; Struhl & Segal, 2013; Friedman & Rando, 2015; Kubik *et al*, 2017; Lai & Pugh, 2017; Woo *et al*, 2017; Cramer, 2019; Brahma & Henikoff, 2020). TFs are therefore constantly moving off and onto different loci, probing for appropriate interactions, also under conditions of steady-state transcriptional output (Hammar *et al*, 2014). The rates with which proteins interact with DNA, their on- and off-rates, dictate the outcome of all kinds of regulatory programs. Understanding how DNA-dependent processes work at the molecular level therefore requires methods to measure the dynamics of protein-DNA binding interactions in a systematic manner.

Different methods have been applied to investigate protein-DNA interaction dynamics. Initial *in vitro* measurements showed very stable TF-DNA binding that could last for more than an hour (Perlmann *et al*, 1990; Hoopes *et al*, 1992). This view was challenged by *in vivo* measurements showing much more dynamic interactions (Hager *et al*, 2009; Larson, 2011; Mueller *et al*, 2013; Voss & Hager, 2014; Coleman *et al*, 2015; Brignall *et al*, 2019; Elf & Barkefors, 2019), likely in part due to the presence of nucleosomes (Luo *et al*, 2014; Donovan *et al*, 2019a; Mivelaz *et al*, 2020). Direct visualisation of protein-DNA interaction dynamics by fluorescence microscopy has been pivotal in forming the current view that binding of many proteins is indeed highly dynamic (McNally *et al*, 2000; Elbi *et al*, 2004; Karpova *et al*, 2004; Stavreva *et al*, 2004; Bosisio *et al*, 2006; Yao *et al*, 2006; Karpova *et al*, 2008; Kloster-Landsberg *et al*, 2012). These studies have also been crucial for showing the importance of dynamics and how this can be regulated through distinct mechanisms. A drawback of microscopy is scope however. Information is provided for only part of the nucleus collectively, or only for a single locus. It would be very useful to determine interaction dynamics at many different binding sites individually, preferably across an entire genome.

Genome-wide protein-DNA binding can be measured by chromatin immunoprecipitation (ChIP) *in vivo* (Gilmour & Lis, 1984; Kuo & Allis, 1999; Park, 2009; Collas, 2010; Furey, 2012). On its own, ChIP only provides a static indication of the degree of binding during the time-window of protein-DNA cross-linking. ChIP cannot measure protein-DNA binding dynamics directly. Competition ChIP is a ChIP variant that uses inducible switching between two differentially tagged isoforms of the same protein and has been applied to measure turnover of nucleosomes and TFs (Dion *et al*, 2007; Rufiange *et al*, 2007; van Werven *et al*, 2009; Lickwar *et al*, 2012; Hasegawa & Struhl, 2019). Although limited by the induction kinetics of the competing isoform, competition ChIP has nevertheless highlighted the advantage of determining dynamics at different loci in a genome-wide manner. It has revealed differences in dynamics between promoter classes, differences in nucleosome turnover between promoters and gene bodies and showed that

differential TF turnover at different loci is an important basis of transcription regulation.

Binding dynamics are determined by TF concentrations, and by on- and off-rates. On- and off-rates are two distinct facets of dynamics. Both would be useful to measure separately since they are likely influenced and regulated by different molecular mechanisms. Having both would also enable the estimation of dissociation constants and the binding free energy. A second adaptation of ChIP has indeed focused on determining on-rates by measuring the kinetics of binding during a formaldehyde cross-linking time-course (Poorey *et al*, 2013). As a method, this is still under development (Zaidi *et al*, 2017) and has only been applied to a few binding sites and not genome-wide as yet. Here, we devised a method that directly determines off-rates and does so for all binding sites across a genome. This was achieved by applying anchor-away to rapidly deplete unbound proteins from the nucleus (Haruki *et al*, 2008; Grimaldi *et al*, 2014), thereby removing the on-rate contribution to binding levels. Monitoring the time-dependent decay of protein-DNA binding across all genomic locations results in determination of off-rates, also in the form of locus-specific residence times. The method DIVORSEQ (Determining *In Vivo* Off-Rates by SEQuencing), is applied here to Abf1, a *Saccharomyces cerevisiae* general regulatory factor akin to chromatin pioneering TFs in mammals (Zaret & Carroll, 2011; Kubik *et al*, 2017). Alongside roles in shaping chromatin architecture (Venditti *et al*, 1994; Lascaris *et al*, 2000; Yarragudi *et al*, 2004; Hartley & Madhani, 2009), several different functions have been attributed to Abf1, including involvement in transcription regulation (Gailus-Durner *et al*, 1996), telomere binding (Enomoto *et al*, 1994; Pryde & Louis, 1999), DNA replication (Marahrens & Stillman, 1992), DNA repair (Reed *et al*, 1999) and RNA polymerase II roadblock termination (Roy *et al*, 2016; Candelli *et al*, 2018). Applying DIVORSEQ to Abf1 results in determination of off-rates for 191 different binding sites, with estimated residence times ranging from 4.5 to 37 minutes. Sites with different off-rates are associated with different functional characteristics that include their transcriptional dependency on Abf1, nucleosome positioning and the ability to roadblock RNA polymerase II thereby aiding transcription termination. The results emphasize that off-rate is an important characteristic of TF function and indicate that DIVORSEQ is a useful method for investigating protein-DNA binding dynamics genome-wide.

Results

Nuclear depletion of Abf1

To inducibly remove unbound Abf1 from the nucleus, an Abf1 anchor-away strain (Haruki *et al*, 2008) was created in the *Saccharomyces cerevisiae* BY4742 background (de Jonge *et al*, 2017). Abf1 was tagged with an FK506 binding protein–rapamycin binding (FRB) domain for nuclear depletion, green fluorescent protein (GFP) to monitor cellular localisation and a V5 epitope for ChIP (Southern *et al*, 1991). *ABF1* deletion is lethal (Halfter *et al*, 1989; Rhode *et al*, 1989). To investigate whether tagging of Abf1 interferes with its function, growth of tagged strains was compared to the untagged background. Tagging Abf1 has only a slight effect on growth (**Supplemental Fig S1A**), indicating that tagging does not greatly interfere with Abf1 function, as has been observed before (Kubik *et al*, 2015). Because of its essential nature, cells are expected to cease growth when Abf1 is depleted from the nucleus. Indeed, upon inducing nuclear depletion, cells show a clear disruption of growth, leading to complete growth cessation (**Supplemental Fig S1B**). Because loss of growth is a downstream effect, the rate of growth cessation does not necessarily reflect the speed of nuclear depletion (de Jonge *et al*, 2017). To directly visualize depletion, cellular localisation of Abf1 was monitored using fluorescence microscopy. As expected, nuclear depletion of Abf1 indeed occurs much more rapidly than growth cessation (**Supplemental Fig S1C and S1D**).

Determining *in vivo* off-rates by sequencing: DIVORSEQ

Having ascertained Abf1 depletion, we next determined whether the system can be used to measure TF residence times ($1/k_{off}$) at different sites across the genome. As published elsewhere (de Jonge *et al*, 2019), first the ChIP protocol was extensively optimized at almost all steps, to yield results better comparable between different time-points. Next, to determine off-rates, Abf1 was depleted from the nucleus and its binding levels were measured genome-wide using the optimized ChIP-seq protocol at 11 time-points during 90 minutes of depletion, all in biological triplicate (**Fig 1A**). The binding sites detected before depletion (t=0) correspond well with previously published Abf1 binding sites (Kasinathan *et al*, 2014; Zentner *et al*, 2015; Rossi *et al*, 2018b). Over 90% of binding sites overlap with previously reported sites (**Supplemental Fig S2A**). As exemplified, different genomic locations show distinct rates of binding peak decay (**Fig 1B**), indicating different Abf1 residence times at these sites. Quantification and fitting the exponential decay model (**Fig 1A**) to the data (**Fig 1C-1E**), yields an estimated site-specific off-rate that can also be expressed as an average TF residence time for that site. The examples (**Fig 1B-1E**) were chosen to cover the wide range of different off-rates/residence times observed. After stringent peak filtering to obtain only reliable signals (Materials and Methods), off-rates and the corresponding residence times were obtained for 191 Abf1 binding sites by fitting exponential decay models to the ChIP-seq data of each individual binding peak. Almost all models closely match the actual binding data, with low residuals (**Supplemental Fig S2B**) and a

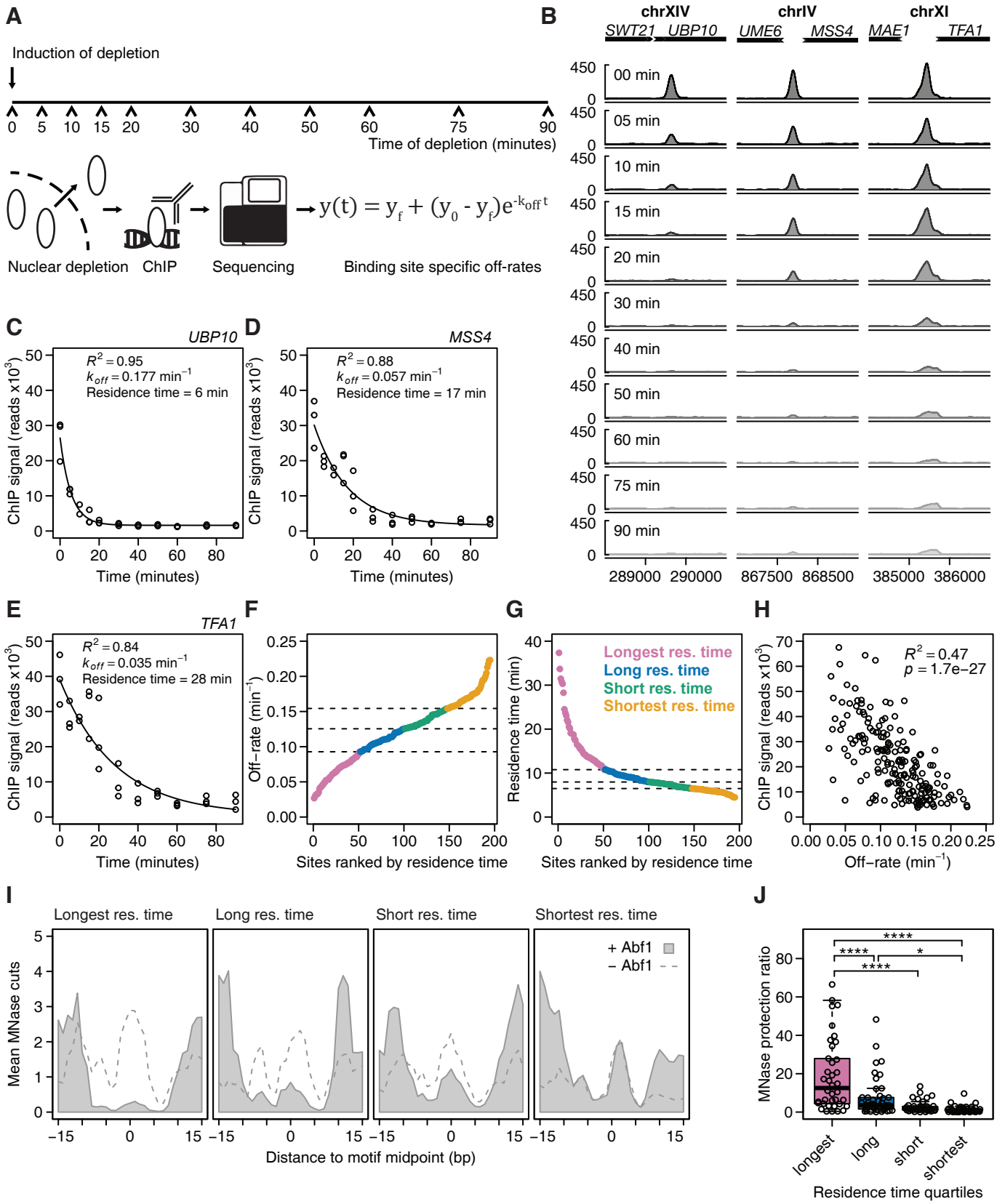

Figure 1. DIVORSEQ measures distinct residence times at different genomic sites.
(A) Schematic overview of the DIVORSEQ method. Unbound protein of interest is depleted from the nucleus and at several time points during the depletion, binding levels are measured using ChIP-seq. The decrease in binding levels is fitted using an exponential decay model and off-rates and residence times are estimated for all binding sites across the genome. **(B)** Abf1 binding during the depletion time course at three Abf1 binding sites with different rates of binding decrease. The signal at each time point is the average of three biological replicates, except for the 10 minutes time point, where one time point was discarded. **(C-E)** Fit of the exponential decay model for the examples shown in (B). The estimates for off-rates, residence time and goodness of fit are

(legend continued on next page)

median R^2 of 0.95 (**Supplemental Fig S2C,** lowest R^2 = 0.63). Based on these models the off-rates for Abf1 range between 0.027 and 0.23 min^{-1} (**Fig 1F**). This corresponds to a residence time of 4.5 minutes for the most dynamic Abf1 sites, the divergent promoter of *SRB2* and *NCP1*, and a residence time of 37 minutes for the promoter of *OCA5* which has a very stable Abf1 binding peak (**Fig 1G**). This is the first indication that DIVORSEQ can measure residence times over a considerable range and that Abf1 has distinct residence times at different locations across the genome.

DIVORSEQ-derived TF residence times correspond to MNase protection rates

To initially test whether DIVORSEQ-derived off-rates are realistic measures of Abf1 binding stability, two strategies were employed. First, residence times were compared to Abf1 binding at *t*=0. Since off-rates influence steady-state binding levels, some degree of correspondence is expected. There is indeed correlation between the DIVORSEQ-derived off-rates and binding levels (**Fig 1H**), whereby sites with low off-rates have higher Abf1 binding levels. That the correspondence is not complete is also expected because on-rate contributes to steady-state binding levels as well. These results therefore also indicate that the relative importance of on- and off-rates may differ for different genomic binding sites. A second verification of the DIVORSEQ-derived off-rates was therefore also sought. This was based on an independently generated MNase cleavage dataset, derived from a strain expressing free MNase (Kubik *et al*, 2018). Since it is well known that TF occupancy can result in protection against MNase cleavage, it is expected that Abf1 binding sites with the lowest off-rate should show the highest degree of MNase protection. This is indeed the case. Abf1 binding sites were divided into the four quartiles with the longest, long, short and shortest Abf1 residence times (**Fig 1F and 1G**). The average MNase cleavage is plotted for each quartile relative to the Abf1 binding motif (**Fig 1I**, grey area) and is indeed seen to increase in the four quartiles from left (longest residence times, least MNase cleavage) to right (shortest residence times, most cleavage). That protection against MNase cleavage in the quartiles with long Abf1 residence times is indeed dependent on Abf1 is demonstrated by an overall increase in MNase cleavage after prolonged Abf1 depletion (**Fig 1I**, dashed line). The extent of MNase protection is also shown for each individual site in each quartile (**Fig 1J**). DIVORSEQ-derived Abf1 off-rates correspond well to the degree of MNase protection. This indicates that the method performs as designed and provides meaningful data for a wide range of TF binding stabilities at different locations across the genome.

Increased Abf1 binding stability is associated with larger nucleosome free regions

Having established that the DIVORSEQ-derived off-rates are meaningful reflections of binding stability, we next asked whether there are mechanistic relationships between stability as measured in this manner and the roles of Abf1. Abf1 is important for shaping local chromatin architecture (Venditti *et al*, 1994; Lascaris *et al*, 2000; Yarragudi *et al*, 2004; Hartley & Madhani, 2009; Ganapathi *et al*, 2011; Krietenstein *et al*, 2016; Kubik *et al*, 2018) and contributes to the creation of nucleosome free regions (NFRs) by competing with nucleosomes and acting as a barrier that chromatin remodellers use to position surrounding nucleosomes. To investigate whether Abf1 binding stability is related to its role in creating NFRs, nucleosome positioning data (Kubik *et al*, 2015) was investigated in the context of different Abf1 residence times. Sites with more stable Abf1 binding (longer residence times, **Fig 2**, top) have larger NFRs (308 bp) compared to sites with shorter residence time sites (**Fig 2**, bottom, 272 bp). These results obviously fit well with the idea that more stably bound Abf1 can more efficiently repel nucleosomes. However, this does not rule out the converse whereby nucleosome remodelling and nucleosome competition causes increased Abf1 off-rates at those sites with reduced residence times. Most importantly for the goals of our study, alongside the MNase protection data (**Fig 1I and 1J**), the NFR-size associated differences shows that DIVORSEQ-derived Abf1 off-rates can be functionally meaningful in this manner too.

Changes in mRNA synthesis rates match Abf1 binding dynamics

We next investigated whether Abf1 binding dynamics play a role in the function of Abf1 as a transcriptional regulator (Buchman & Kornberg, 1990; Gailus-Durner *et al*, 1996; Miyake *et al*, 2002, 2004; Yarragudi *et al*, 2007; Paul *et al*, 2015; Kubik *et al*, 2018). Previous studies have shown that not all Abf1 bound promoters show

shown in the plots. **(F and G)** Distribution of the off-rates (F) or residence times (G) of the 191 binding sites ranked by decreasing residence time. The four different residence time quartiles are highlighted with different colours. **(H)** Relationship between Abf1 binding levels before depletion and off-rates for the 191 Abf1 binding sites. **(I)** Average *in vivo* MNase sensitivity of the residence time quartiles, plotted as the average number of MNase cuts at each position relative to the Abf1 binding motif (MacIsaac *et al*, 2006) before (grey fill) or after (dashed line) nuclear Abf1 depletion. The data were smoothed using a 3 bp window. **(J)** Extent of MNase protection by Abf1 for each residence time quartile. The MNase protection ratio is the mean number of cuts in the region protected by Abf1 (-8 bp until +8 bp) after depletion of Abf1 (I, dashed line), divided by the mean number of cuts in the same region before depletion (I, light grey fill). Asterisks denote a significant difference between the quartiles, calculated using a one-way ANOVA followed by Tukey's honest significant difference (HSD) test (* $p < 0.05$ and **** $p < 0.0001$).

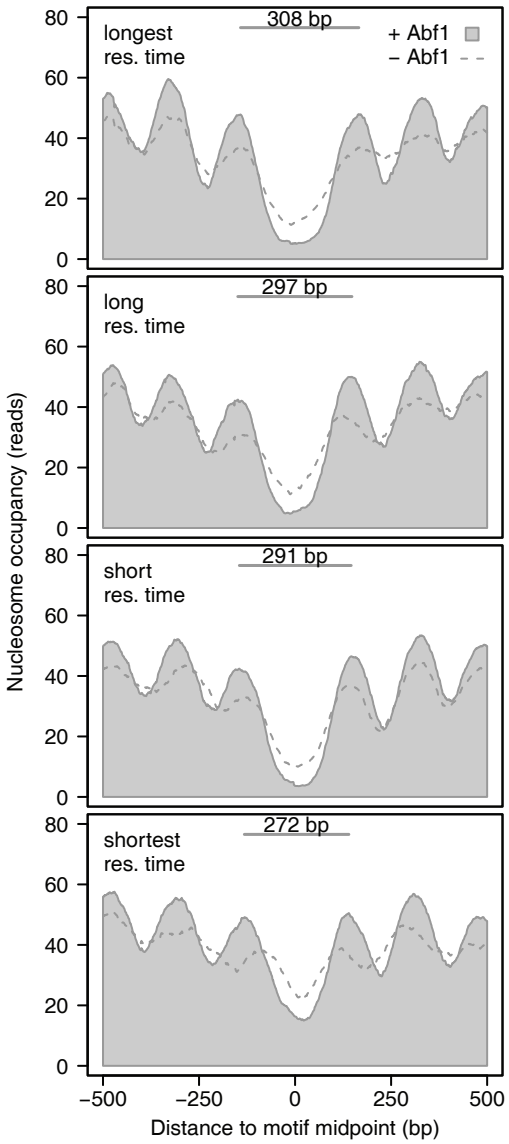

Figure 2. Nucleosomes architecture corresponds to residence times

Average nucleosome occupancy of the residence time quartiles before (light grey fill) and after (dashed line) Abf1 depletion, centred on the Abf1 binding motif. Nucleosomes of all residence time quartiles reposition upon Abf1 depletion, which indicates that Abf1 contributes to the positioning of nucleosomes for all quartiles. The average distance between the midpoints of the -1 and +1 nucleosomes before depletion of Abf1 are indicated for each quartile. Nucleosome binding data are from (Kubik *et al*, 2015).

transcriptional dependency on Abf1 (Schroeder & Weil, 1998; Yarragudi et al, 2007; Paul et al, 2015). This has been ascribed to either lower inherent propensity for nucleosome formation at some sites, binding too far away from a transcription start site, or redundancy with other TFs (Paul *et al*, 2015; Kubik *et al*, 2018). We therefore first determined which genes are dependent on Abf1 by measuring mRNA synthesis rates genome-wide using 4-thiouracil labelling of nascent transcripts (Sun *et al*, 2012) during a 90 minute Abf1 depletion time-course, at the same times points that were used to determine off-rates (**Fig 3A**). Approximately half of the genes with Abf1 promoter binding show a decrease in mRNA synthesis rates upon Abf1 depletion, in agreement with what has previously been described for Abf1 (Schroeder & Weil, 1998; Yarragudi *et al*, 2007; Paul *et al*, 2015). The non-responsive genes show little, if any, concomitant change in nucleosome repositioning (**Fig 3B**), also in agreement with previous studies (Kubik *et al*, 2018). The set of genes that do show Abf1-dependency were next used to investigate the role of binding dynamics.

First, steady-state synthesis rates (transcripts per minute per cell, Sun *et al*, 2012) were compared to steady-state binding levels of Abf1. In contrast to what might be expected, there is virtually no relationship between the amount of Abf1 at a promoter and promoter activity at steady-state (**Fig 3C**). Regardless of absolute binding levels, promoters with more stably bound Abf1 also do not show higher synthesis rates (**Fig 3D**). There is however some association between the steady-state amount of bound Abf1 and the early changes in synthesis rates observed upon Abf1 depletion (**Fig 3E and supplemental Fig S3A**). The relationship between Abf1 presence and transcriptional dependency is markedly stronger when taking into account the DIVORSEQ-derived off-rates (**Fig 3F and supplemental Fig S3B**). Genes showing the largest change in promoter output are those with the highest off-rates. This holds both for the 10 minute time-point analysed in **Fig 3F,** as well as when fitting an exponential decay model to the entire mRNA synthesis rate time-course (**Fig 3G**). For those genes that are dependent on Abf1 for transcriptional activity, there is a strong correspondence between the loss of Abf1 and the reduction in synthesis rate. The relationship between Abf1 and transcriptional output only becomes clear when plotting off-rates (**Fig 3F and 3G**). This emphasizes the importance of methods to investigate interaction dynamics genome-wide and the utility of DIVORSEQ for this purpose. As discussed later, our analyses agree with the idea that an Abf1-dependent NFR is the most important determinant for setting up transcription, resulting in associated dependencies on Abf1 (Paul *et al*, 2015; Kubik *et al*, 2018; **Fig 3B**), but that fine-tuning the absolute levels of steady-state transcriptional output is further dependent on other contributing transcription (co-)factors.

Stably bound sites are more efficient roadblocks for pervasive Pol II transcription

In addition to being a chromatin organizer, Abf1 has been shown to function as roadblock for pervasive transcription (Roy *et al*, 2016; Candelli *et al*, 2018). In this role, Abf1, like the other general regulatory factors Reb1 and Rap1, can block transcribing RNA polymerase II (Pol II). This collision causes Pol II to stall, to become ubiquitinylated and likely degraded (Colin *et al*, 2014; Candelli *et al*, 2018). An obvious hypothesis, as has indeed been suggested (Roy & Chanfreau, 2018), is that TF binding stability may

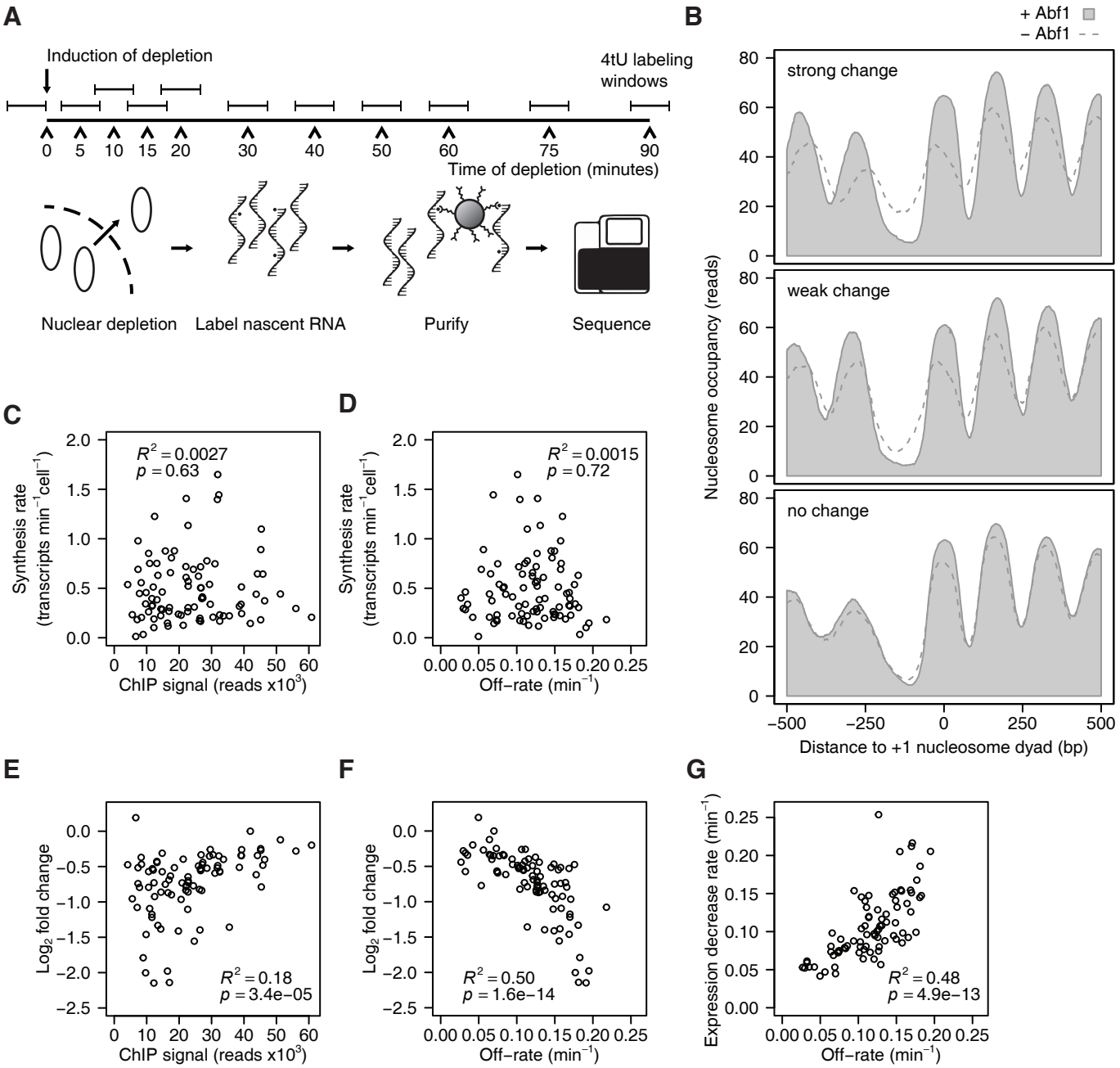

Figure 3. Dynamics of mRNA synthesis changes follow the dynamics of Abf1 dissociation.
(A) Schematic overview of the experiment set-up for measuring promoter output dynamics by labelling nascent RNA. The protein of interest is depleted from the nucleus and nascent RNA is labelled for 6 minutes using 4-thiouracil (4tU) at several time points during the depletion. Total RNA is extracted, nascent RNA is purified by biotinylating 4tU labelled RNA and the purified RNA is sequenced. Samples were taken such that the centre of the labelling period was the same as the time points that were used for DIVORSEQ. **(B)** Average nucleosome occupancy relative to +1 nucleosome dyad, of genes with Abf1 binding to the promoter that show strong changes (fold change > 2 at *t*=20, top panel, *n*=44), weak changes (1.5 ≤fold change ≤ 2 at *t*=20, middle panel, *n*=42) or no changes (fold change < 1.5 at *t*=20, bottom panel, *n*=112) in mRNA synthesis upon Abf1 depletion. Nucleosome occupancy is shown before (light grey fill) and after (dashed line) Abf1 depletion. Nucleosome binding data and +1 nucleosome positions are from (Kubik *et al*, 2015). Downregulated and Abf1 bound genes without an annotated +1 nucleosome were omitted from the plots. **(C and D)** Relationship between steady state synthesis rates (Sun *et al*, 2012) and binding levels before depletion (C), or off-rates (D). Genes are shown that are Abf1 bound and downregulated (fold change > 1.5 and $p < 0.01$ at 20 and 30 minutes of depletion, yielding 88 genes) and have available synthesis rates (*n*=87). **(E and F)** Relationship between $\log_2$ mRNA synthesis rate changes after 10 minutes of depletion and binding levels before depletion (E) or off-rates (F). Genes are shown that are Abf1 bound and downregulated (fold change > 1.5 and $p < 0.01$ at 20 and 30 minutes of depletion, *n*=88). **(G)** Relationship between expression decrease rates of downregulated genes and off-rates of the corresponding Abf1 binding site. The expression decrease rates were calculated by fitting the 4tU-seq time data course using the same exponential decay model that was used for the off-rates. The genes from (E and F) are shown, except for the ones where the 4tU-seq data could not be fitted with an exponential decay model (*n*=82).

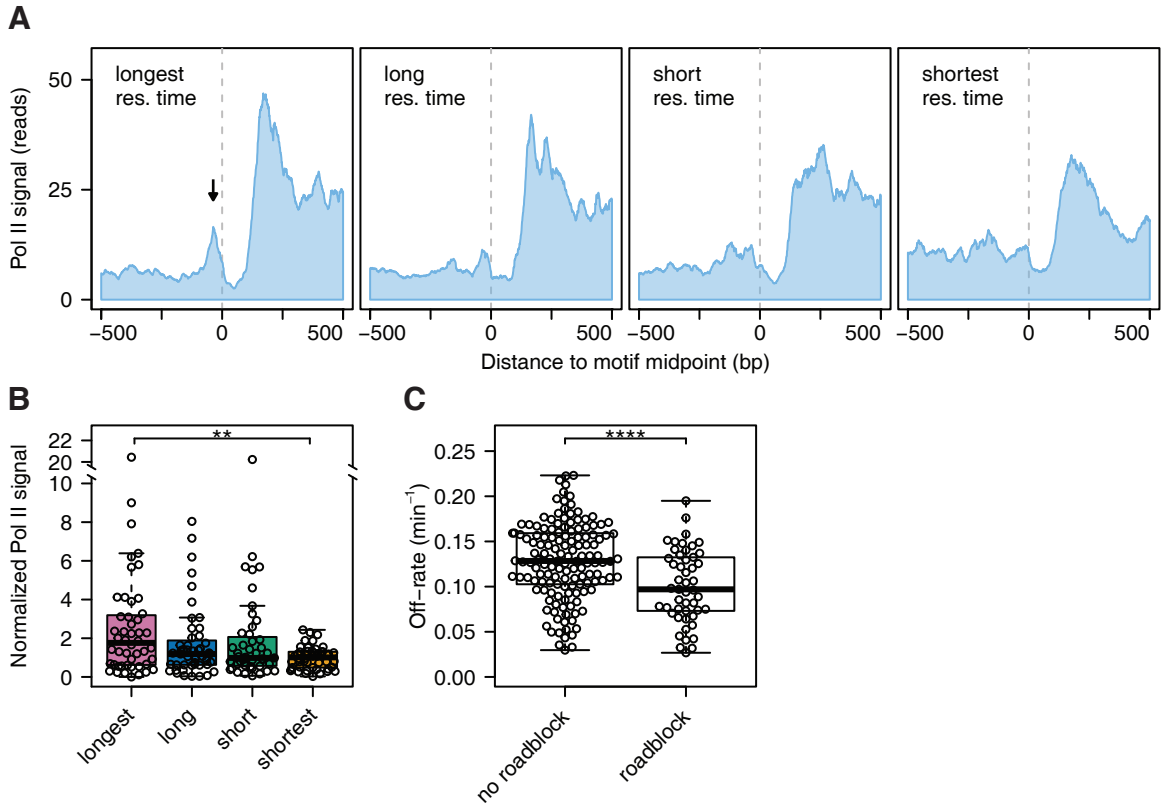

Figure 4. Sites with long residence times function as a roadblock for pervasive transcription
(A) Average RNA polymerase II binding for the different residence time quartiles. Binding profiles are centred on the Abf1 motif. The dotted line marks the midpoint of the Abf1 motif. All RNA polymerase II binding data were reoriented such that each motif is oriented in the same direction. RNA polymerase II binding is PAR-CLIP (photoactivatable ribonucleoside-enhanced cross-linking and immunoprecipitation) data from (Schaughency *et al*, 2014). **(B)** Quantification, by residence time quartile, of normalized Pol II binding levels at the roadblock peak. These levels are defined as the amount of roadblocked Pol II (located at -37 ± 5 bp) divided by the amount of upstream Pol II (from -300 to -100 bp). Asterisks denote a significant difference between the quartiles, calculated using a one-way ANOVA followed by Tukey's HSD test (** $p < 0.01$). **(C)** Difference in off-rates between sites that are a roadblock (normalized Pol II signal > 2) and those that are not. The *p*-value was calculated using a two-tailed t-test (**** $p < 0.0001$).

contribute to roadblock function. To test this idea, data of actively transcribing Pol II (Schaughency *et al*, 2014) was analysed. The average Pol II presence relative to the Abf1 binding motif was plotted for each of the residence time quartiles (**Fig 4A**). A roadblock peak (**Fig 4A**, arrow) can be observed immediately upstream of the Abf1 motif for the quartile with the longest residence times, and this becomes less pronounced with shorter residence times. Quantification of roadblock efficiency at each individual site confirms that stronger roadblocks are observed in the quartile with the longest residence times (**Fig 4B**). In agreement with this, sites with stalled Pol II have significantly lower off-rates compared to sites that do not (**Fig 4C**). More stably bound Abf1 is a more efficient roadblock for transcribing Pol II, further demonstrating the utility of genome-wide off-rate measurements for molecular mechanistical understanding.

Factors contributing to Abf1 binding stability

When applied to Abf1, DIVORSEQ indicates that there is a considerable range of off-rates and that this contributes to different aspects of Abf1 function. The ability to determine residence times also allows for investigation into the factors that determine different off-rates. The DNA binding motif is obviously an important factor for determining Abf1 binding stability. To evaluate the contribution of motif frequency, the number of Abf1 motifs in the vicinity of each Abf1 peak was counted. Although there are only a few peaks with multiple motifs, it is clear that most sites with more than one Abf1 binding motif have significantly longer residence times compared to sites with only a single binding motif (**Fig 5A**). Such increases in stability are likely caused by different types of cooperative effects associated with the presence of multiple motifs (Adams & Workman, 1995; Polach & Widom, 1996; Miller & Widom, 2003; Hager *et al*, 2009; Mirny, 2010).

Beside the number of motifs, the sequence composition of the binding motif is also likely to contribute to binding stability. To investigate how motif composition affects Abf1 binding stability, the motif score of each of the binding motifs was compared between the residence time groups. Binding sites with the longest residence time have a motif that is closer to the consensus compared to the other sites (**Fig 5B**),

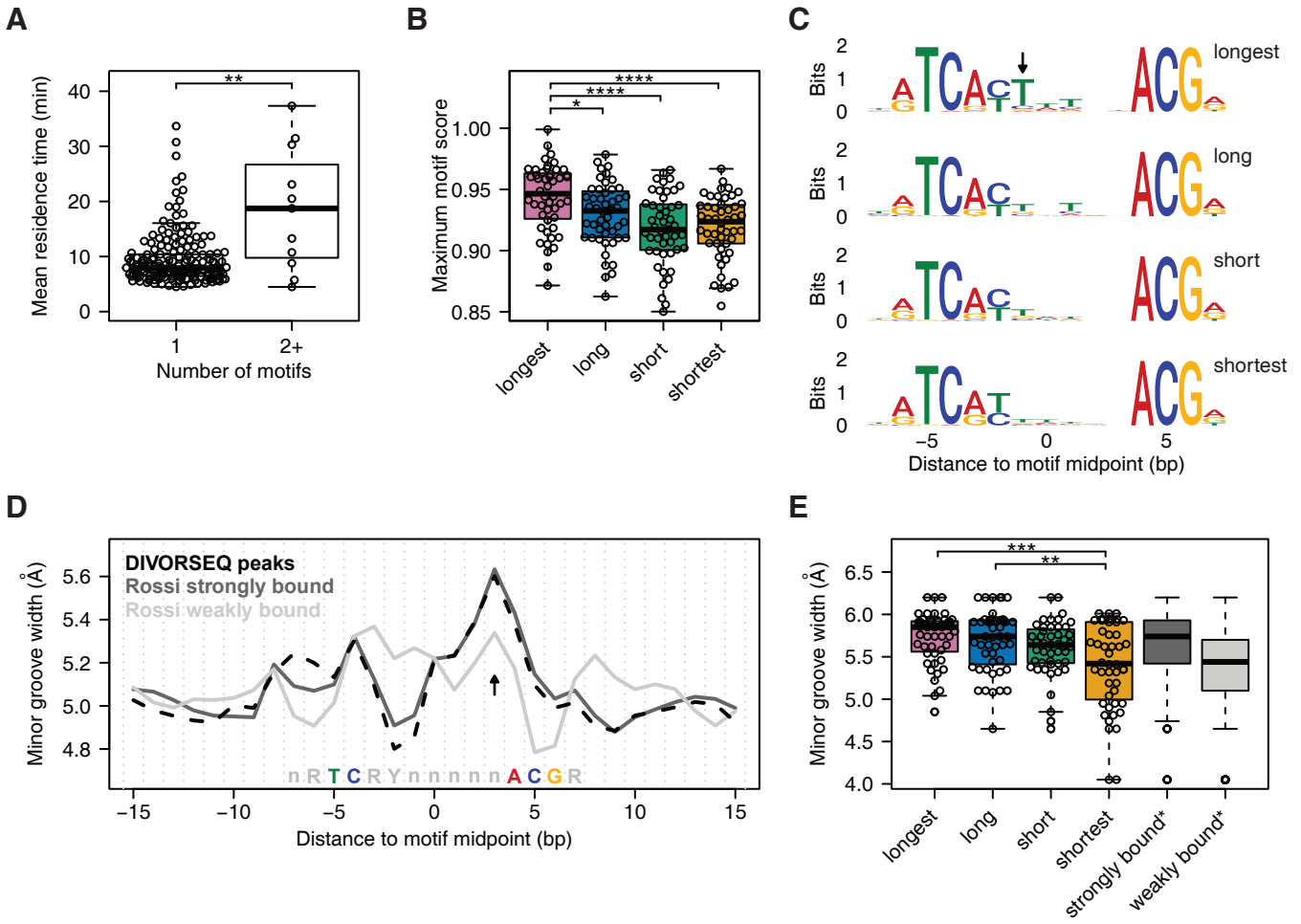

Figure 5. Factors that contribute to Abf1 binding stability.
(A) Difference in residence times between sites with one motif and sites with two or more motifs. The p-value was calculated using a Wilcoxon rank-sum test (** $p = 0.0011$), rather than a t-test ($p = 0.0081$) as used in **Fig 4C,** since the group with 1 binding motif is not normally distributed. **(B)** Difference in maximum motif score between the different residence time quartiles. When a site has more than one motif, the highest score was used. **(C)** Sequence logos showing the representative binding motif of each residence time quartile. Motifs from the longest residence time quartile are enriched ($p = 0.0046$) for having a thymine at position -1 bp (arrow). **(D)** Predicted minor groove width centred at the Abf1 binding motif of all 191 Abf1 sites found here (black, dashed line) and Abf1 binding motifs defined as strongly bound (dark grey line) and weakly bound (light grey line) by (Rossi *et al*, 2018a). **(E)** Difference in predicted minor groove width between the residence time quartiles at position +3 bp from the motif midpoint (D, arrow). In addition, the minor groove width at this position of the Abf1 motifs defined as strongly and weakly bound by (Rossi *et al*, 2018a) are shown (n=400 for each group). Asterisks in (B) and (E) denote adjusted p-values calculated using a one-way ANOVA followed by Tukey's HSD test between the residence time quartiles (* $p < 0.05$, ** $p < 0.01$, *** $p < 0.001$, **** $p < 0.0001$).

which indicates that having a stronger binding motif leads to more stable binding. Indeed, mutating the binding site of another well-studied TF, Gal4, results in a shorter residence time (Donovan *et al*, 2019b). To investigate the contribution of motif sequence to Abf1 binding stability in more detail, the consensus motifs of the different residence time groups were compared to each other (**Fig 5C**). Although the consensus motifs of all four groups are similar, showing good correspondence to published motifs (MacIsaac *et al*, 2006; Kasinathan *et al*, 2014; Zentner *et al*, 2015; Rossi *et al*, 2018a), the longest residence time group has a significant enrichment (p = 0.0046) for a thymine in the variable part of the motif, at position -1 bp (**Fig 5C**, arrow). This suggests that having a thymine at this position is not needed for binding per se, but that it contributes to the binding stability of Abf1. In agreement with this, mutation of a thymine residue at this position reduces the binding levels of Abf1 *in vitro* (Gailus-Durner *et al*, 1996).

DNA shape can also influence Abf1 binding levels (Zentner *et al*, 2015; Rossi *et al*, 2018a). Strongly and weakly bound Abf1 sites differ in their predicted minor groove width as estimated across naked DNA motifs (Rossi *et al*, 2018a). The Abf1 sites found here closely resemble the strongly bound sites in their minor groove width pattern (**Fig 5D**). Strikingly, the same analysis performed across the four groups of sites with different residence times reveals that in terms of minor groove width at position +3 bp (**Fig 5D**, arrow), the group with shortest Abf1 residence times most closely resembles the

sites with low Abf1 binding levels (Rossi *et al*, 2018a), in having a smaller minor groove (**Fig 5E**). This suggests that the lower binding levels observed on sites with a reduced minor groove width at the +3 position is caused by a higher off-rate. The extended genome-wide survey of Abf1 binding stabilities demonstrates that factors influencing TF binding stability *in vivo* can also be advantageously studied by DIVORSEQ.

Discussion

The dynamics of proteins interacting with DNA are thought to play an important role in the regulation of chromatin-associated processes such as transcription (Hager *et al*, 2009). To fully understand these processes at a molecular level requires an understanding of the underlying binding dynamics. DIVORSEQ quantifies protein-DNA binding dynamics *in vivo* by directly measuring off-rates and residence times at multiple binding sites across an entire genome. Applying DIVORSEQ to the TF Abf1 shows that the method can measure meaningful differences in off-rates spanning a wide range of values. Our results show how motif number, sequence and structure of the binding motif contribute to off-rates and how this aspect of binding dynamics influences the roles of Abf1 as a chromatin organizing factor, a transcriptional regulator and a termination roadblock for RNA polymerase II at different sites across the genome.

Abf1 is a general regulatory factor, known to organize chromatin (Venditti *et al*, 1994; Lascaris *et al*, 2000; Yarragudi *et al*, 2004; Hartley & Madhani, 2009; Ganapathi *et al*, 2011; Krietenstein *et al*, 2016; Kubik *et al*, 2018). Our results show good correspondence between NFR size and binding stability (**Fig 2**). Sites with shorter Abf1 residence times have smaller NFRs. This could either be explained by stronger nucleosome exclusion through more stably bound Abf1, or conversely, by more stable binding of Abf1 in larger NFRs. Abf1 shapes the local chromatin architecture by competing with nucleosomes (Venditti *et al*, 1994; Yarragudi *et al*, 2004) and by acting as a barrier that chromatin remodellers use to position flanking nucleosomes (Krietenstein *et al*, 2016). It seems reasonable that Abf1 forms a more efficient barrier when it is more stably bound, thus repelling nucleosomes more efficiently, which would support the hypothesis that stable binding creates bigger NFRs. On the other hand, being a barrier means that chromatin remodellers actively position nucleosomes towards Abf1. Therefore, nucleosomes that are being positioned by remodellers may exert a force on Abf1 and destabilize its binding. In this hypothesis, competition with nucleosomes could reduce the residence time of Abf1, as has been shown for Rap1 (Lickwar *et al*, 2012; Mivelaz *et al*, 2020). Upon depletion of Abf1, nucleosomes become repositioned in all Abf1 residence time quartiles, but sites with the shortest residence time show the biggest reduction in NFR size (**Fig 2**). This fits with nucleosome positioning leading to shorter Abf1 residence times at these sites. Neither hypothesis can, nor need be excluded as yet. The observed correspondence between NFR size and Abf1 off-rates at different sites highlights the advantage of such measurements as a starting point for detailed characterisation of molecular mechanisms.

Besides organizing chromatin, Abf1 also functions as a transcriptional regulator (Buchman & Kornberg, 1990; Gailus-Durner *et al*, 1996; Miyake *et al*, 2002, 2004; Yarragudi *et al*, 2007). Abf1 is known to be only a weak activator of transcription (Buchman & Kornberg, 1990; Levo *et al*, 2017) and the results presented here indicate that it mainly regulates transcription through repositioning nucleosomes, which is consistent with previous reports (Paul *et al*, 2015; Kubik *et al*, 2018). Our results fit with Abf1 stimulating transcription by creating an NFR that allows other regulatory factors to bind and whose activities may more directly dictate steady-state expression levels. This offers an explanation for why there is little correlation between steady-state mRNA synthesis rates and Abf1 binding levels or off-rates (**Fig 3C and 3D**), but nevertheless good correlation between off-rates and changes in mRNA synthesis rates upon depletion (**Fig 3F**). Removal of Abf1 causes NFR collapse for those promoters that have no redundant mechanisms of NFR upkeep (**Fig 3B**), resulting in cessation of promoter activity. This is in contrast to Rap1, which is known to directly contact TFIID (Garbett *et al*, 2007) and may directly recruit the transcription pre-initiation complex itself. Such direct recruitment suggests that Rap1 is the main regulator of transcription of its targets, explaining correlation between Rap1 binding dynamics and steady-state mRNA synthesis levels (Lickwar *et al*, 2012). As with the analysis of roadblock function for Abf1, different modes of regulator activity or function may therefore be revealed by detailed analyses of binding dynamics.

A limitation of DIVORSEQ is that analysis is in bulk, rather than at the single cell resolution available through microscopy (Hager *et al*, 2009; Larson, 2011; Mueller *et al*, 2013; Voss & Hager, 2014; Coleman *et al*, 2015; Brignall *et al*, 2019; Elf & Barkefors, 2019). This is offset by the advantage of determining off-rates for many loci across the genome in parallel. Other methods that measure site-specific *in vivo* binding dynamics include competition ChIP, which determines turn-over and is limited by a slow induction of the competitor protein, as well as by the substantial carbon source perturbation required for induction (Schermer *et al*, 2005). DIVORSEQ directly measures off-rates and has been designed for application alongside on-rate measurement by cross-linking kinetic analyses (Poorey *et al*, 2013), that has yet to be applied at the genomic scale (Zaidi *et al*, 2017). Considerations that need to be made when applying DIVORSEQ include having sufficiently rapid removal of unbound proteins from the nucleus. Using anchor-away (Haruki *et al*, 2008), an estimated 2,000 molecules can be depleted from the nucleus per minute (Warner, 1999). This implies that for

highly abundant proteins such as Abf1, with an estimated 6,000 molecules (Ho *et al*, 2018), residence times will be determined at minute-scale resolution. That anchor-away is sufficiently rapid for Abf1, is indicated by the excellent fit to first-order kinetics observed and the wide range of different off-rates obtained. Besides anchor-away, other techniques that facilitate nuclear depletion could also be used (Klemm *et al*, 1997; Bayle *et al*, 2006; Busch *et al*, 2009), contingent on rapidity. A second consideration is that the ChIP or genomic location protocol requires results that are comparable between time points. Here we first extensively optimized almost all ChIP protocol steps to achieve this (de Jonge *et al*, 2019). Some limitations still remain. Abf1 can only be cross-linked to sites with a guanine or cytosine at -8 bp from the binding motif centre (Rossi *et al*, 2018a). Sites without a guanidine or cytosine at this position were therefore excluded here although some nevertheless yielded low signals, likely caused by small amounts of cytosolic Abf1 rebinding during the ChIP procedure. Combined with peak filtering for robust binding, this reduced the number of Abf1 sites for which off-rate could be determined. Improvements to DIVORSEQ could therefore be aimed at preventing rebinding and/or applying assays that do not depend on cross-linking (Zentner *et al*, 2015; Skene & Henikoff, 2017). These considerations aside, that the determined off-rates are accurate is corroborated by the MNase protection levels at Abf1 sites with different off-rates, as well as by the diverse aspects of previously established Abf1 function presented here for the first time in the context of a large number of genomic binding sites and their binding dynamics.

Materials and Methods

Strains

The strains used in this study are *Saccharomyces cerevisiae* anchor-away strains (Haruki *et al*, 2008) that were recreated in the BY4742 background (de Jonge *et al*, 2017). Besides the FRB domain from mammalian target of rapamycin (mTOR), the anchor-away tag consists of yeast enhanced green fluorescent protein (yEFGP) and a triple V5 tag. The parental BY4742 anchor-away strain, which has an *FPR1* deletion and a *tor1-1* mutation to desensitize the strain to rapamycin, was used as a wildtype control.

Growth conditions

Strains were streaked from -80°C stocks on appropriate selection plates (for the parental anchor-away strain: YPD + Nourseothricin and for the Abf1-aa strains: YPD + Nourseothricin + Hygromycin), and incubated at 30°C for 3 days. In the morning, liquid pre-cultures were inoculated in 1.5 ml of synthetic complete (SC) medium: 2 g/l dropout mix complete and 6.71 g/l yeast nitrogen base without amino acids, carbohydrate & w/AS (YNB) from US Biologicals (Swampscott, USA) with 2% D-glucose. In the afternoon, several pre-cultures were combined, diluted to final volume of 20 ml and grown overnight. The growth conditions were identical for all experiments and pre-cultures: in SC medium at 30°C, with shaking (230 rpm).

Anchor-away depletion

At *t*=0, Abf1 was depleted from the nucleus by addition of rapamycin (LC Laboratories #R-5000; dissolved to 2 mM in DMSO), to a final concentration of 7.5 µM. For the *t*=0 time point, the same volume of DMSO instead of rapamycin was added and incubated for 90 minutes.

Chromatin immunoprecipitation

ChIP was performed as described in detail in (de Jonge *et al*, 2020) using biological triplicates. To summarize: cells were diluted in the morning to an optical density (OD) of 0.11-0.15 (WPA Biowave CO8000 Cell Density Meter) in 100 ml of SC medium, and grown for at least 2 doublings to an OD_{600} = 0.8, which corresponds to about 2 x 10^7 cells per ml. Additions of rapamycin and DMSO were staggered such that all time points were ready at the same OD (0.8). When this OD was reached, the cells were cross-linked for 5 minutes by addition of 37% formaldehyde (Sigma-Aldrich #252549) to a final concentration of 2%. The formaldehyde was quenched using a final concentration of 1.5M of Tris (tris(hydroxymethyl)aminomethane) for 1 minute. Subsequently, the cells were pelleted by centrifugation at 3220g at 4°C for 3 minutes. The pellet was washed in 10 ml TBS (150 mM NaCl, 10 mM Tris pH 7.5) and pelleted again at 3220g for 3 minutes at 4°C. After resuspension in 1 ml MQ, cells were centrifuged at 3381g for 20 seconds at room temperature and the pellet was snap-frozen in liquid nitrogen and stored at -80°C.

To lyse cells, the cells were resuspended in FA lysis buffer (50 mM HEPES-KOH pH 7.5, 150 mM NaCl, 1 mM EDTA pH 8.0, 1% Triton X-100, 0.1% Na-deoxycholate, 0.1% SDS) containing the protease inhibitors aprotinin, pepstatin A, leupeptin and PMSF to a final volume of 2ml, transferred to 2-ml screw-cap tubes and disrupted using zirconium/silica beads 0.5 mm (BioSpec Products, #11079105z) by bead beating 7 times 3 minutes in a Genie Disruptor (Scientific Industries). The lysate was recovered and centrifuged at 1503g for 2 minutes at 4°C to remove cell debris. The supernatant was subsequently fragmented by sonicating the samples for 10 cycles of 15 seconds on, 30 seconds off using a Bioruptor Pico sonicator (Diagenode #B01060010).

For the immunoprecipitation, 450 µl of the fragmented chromatin was incubated with 1 µl of anti-V5 antibody (Life Technologies #R96025) for 2 hours at 4°C. A 20 µl aliquot was kept separate as an input control. The chromatin + antibody were subsequently bound for 20 minutes at room temperature to magnetic beads

(Dynabeads protein G, Life Technologies #10004D) that were pre-incubated with BSA. The beads were washed twice with PBS and twice using PBS-T. During the last wash, the beads were transferred to fresh LoBind tubes (Eppendorf #0030108051). Cross-links were reversed by incubating in TE/1% SDS (10 mM Tris pH 8.0, 1 mM EDTA pH 8.0, 1% SDS (w/v)) overnight at 65°C. The next morning, RNA was degraded by addition of RNAse A/T1 (Thermo Scientific #EN0551) at 37°C, and subsequently proteins were digested by addition of proteinase K (Roche #03115852001) at 37°C. After protein digestion, DNA was recovered using a Qiagen PCR purification cleanup kit (Qiagen #28106) by eluting in 30 µl buffer EB.

RNA labelling and extraction

For the 4tU-seq time course, 20 ml cultures were used, with biological triplicates for each time point. Rapamycin and DMSO additions were staggered such that all cultures were ready at the same OD (0.8). WT samples incubated with rapamycin or DMSO for 90 minutes were taken along as a controls. Three minutes before the cultures were ready, 4-thiouracil (4tU; Sigma-Aldrich #440736) was added to the cell cultures to a final concentration of 5 mM. Cells were incubated with 4tU for 6 minutes in total, such that the centre of the labelling period matched the time point of the ChIP time course. Subsequently, cells were harvested by centrifugation at 3220g for 3 minutes, cell pellets were snap frozen immediately in liquid nitrogen and stored at -80°C.

To isolate total RNA, cells were resuspended in Acid Phenol Chloroform (Sigma #P1944) and immediately mixed with the same volume of TES buffer (10 mM Tris pH 7.5, 10 mM EDTA, 0.5% SDS). The samples were vortexed hard for 20 seconds, the tubes were covered in aluminium foil to keep the samples dark, and incubated in a 65°C water bath for 10 minutes. Next, the samples were transferred to 1.5 ml tubes and incubated in a thermomixer for 50 minutes at 65°C and 1400 rpm, while covered in aluminium foil. After incubation, samples were centrifuged at 18407g for 20 minutes at 4°C. The water phase was recovered and phenol extraction was repeated once, followed by extraction using chloroform-isoamyl-alcohol (25:1). The RNA was precipitated using sodium acetate (NaAc 3M, pH 5.2) and 100% ethanol (-20°C) by incubating at -20°C for at least 30 min. DTT was also added to a final concentration of 1mM to prevent oxidation of the 4tU. The pellet was washed once with 80% ethanol and resuspended to a final concentration of 1 µg/µl in sterile MQ.

To recover nascent transcripts the protocol from (Dölken *et al*, 2008) was used with minor adaptations. In brief, 100 µg of cleaned RNA was heated to 60°C for 10 minutes and immediately put on ice for 2 minutes. The RNA was biotinylated by adding 200 µl Biotin-HPDP (Thermo Fisher Scientific #21341) dissolved to 1 mg/ml in 30% DMF. Unbound biotin was removed using chloroform extraction. Biotinylated RNA was separated from total RNA using streptavidin-conjugated magnetic beads and µMACs columns (Miltenyi Biotec #130-074-101). The beads were washed 6x using 65°C washing buffer (100 mM Tris pH 7.5, 10 mM EDTA, 1 M NaCl, 0.1% Tween-20) and bound RNA was eluted using 200 µl of 100 mM DTT. The nascent RNA was purified using an RNeasy MinElute Cleanup Kit (Qiagen #74204).

Library preparation and sequencing

ChIP-seq libraries were created using a combination of a NEXTflex Rapid DNA-Seq Kit (Bioo Scientific #NOVA-5144) and a NEXTflex Rapid Directional qRNA-Seq Kit (Bioo Scientific #NOVA-5130) to allow for incorporation of unique molecular identifiers (UMIs) (Kivioja *et al*, 2012) on both sides of each fragment. To improve speed and accuracy, a maximum of 8 libraries were prepared at the same time. To make the amount of starting material of the input samples similar to that of the IP samples, the input samples were diluted 1:300 prior to library prep. End-repair and adenylation were carried using the NEXTflex Rapid DNA-Seq Kit with half of the recommended volumes. The subsequent steps were carried out using the NEXTflex Rapid Directional qRNA-Seq Kit with a quarter of the recommended volumes for the adapter ligation and half volumes for the PCR amplification. The initial volume used for each of the bead clean-ups was adjusted to 50 µl by addition of MQ and bead ratios were kept as recommended. The number of PCR cycles used was the same for all ChIP and input samples (13 cycles) except for the WT IPs where 15 PCR cycles were used. Library yields were assessed using a High Sensitivity DNA bioanalyzer chip (Agilent) and equimolar amounts of library were pooled and sequenced paired-end 2x 75bp on a NextSeq 500 system (Illumina).

4tU-seq libraries were created using the NEXTflex Rapid Directional qRNA-Seq Kit (Bioo Scientific #NOVA-5130) with a slightly modified protocol. During step *D* of the protocol (*i.e.* bead cleanup after second strand synthesis) the beads were resuspended in 10 µl of resuspension buffer, and 8 µl was used for the next step. From this step onwards, half of all recommended volumes were used. The initial volume used for each of the bead clean-ups was adjusted to 50 µl by addition of MQ and bead ratios were kept as recommended. Since the concentrations of labelled RNA differed after the purification, a qPCR was performed to estimate the number of PCR cycles needed for each sample after adapter ligation. The number of cycles that were used varied between 8-12 cycles. Library yields were assessed using a High Sensitivity DNA bioanalyzer chip (Agilent) and equimolar amounts of library were pooled and sequenced paired-end 2x 75 bp in two sequence runs on a NextSeq 500 system (Illumina).

Mapping

Reads from both the ChIP-seq and 4tU-seq experiments

were aligned to the sacCer3 genome assembly (February 2011) using HISAT2 v2.0.5 (Kim *et al*, 2015). The settings for the ChIP-seq samples were "`--add-chrname -X 1000 --score-min L,0,-0.2 -k 1 --no-spliced-alignment -5 12 -3 6`" and for the 4tU-seq samples the settings "`--add-chrname -X 1000 --score-min L,0,-0.175 -5 10 -3 10 --dta -max-intronlen 1500 --rna-strandness RF`" were used. Subsequently, the bam files were filtered to keep only transcripts with a unique combination of UMIs using the custom scripts "addumis2bam.sh" and "uniqify-umis.pl" available from https://github.com/wdejonge/DIVORSEQ.

Peak calling and filtering

The ChIP-seq data was filtered to keep only uniquely mapping reads and subsequently peaks were called using MACS2 v2.1.1.20160309 (Zhang *et al*, 2008) with the settings "`-f BAMPE -g 1.25e7 --keep-dup all --mfold 5 2000 --call-summits -q 0.001 --fe-cutoff 2`" using all three replicate *t*=0 time points (no depletion) versus their corresponding inputs, yielding 948 Abf1 peaks.

To monitor the depletion, the initial binding levels need to be sufficiently strong to accurately measure a reduction in binding levels. Therefore, only binding peaks with a fold enrichment of at least 4 were considered (421 peaks). This also filters out apparent weak binding across open reading frames and tRNAs, which is a known artefact of ChIP (Park *et al*, 2013; Teytelman *et al*, 2013). In addition, it has been recently shown that Abf1 is only efficiently cross-linked to sites with either a guanine or a cytosine at -8 bp from the centre of the Abf1 binding motif (Rossi *et al*, 2018a). For each binding peak, we searched for motifs (± 100 bp from peak summit) that closely match the Abf1 consensus (at least 85% of the consensus motif score from (MacIsaac *et al*, 2006)) and determined whether there was a G/C or an A/T at -8 bp from each motif. Only peaks where all motifs found had a G/C at -8 bp from the motif midpoint were kept for further analysis (195 peaks). Four of these peaks were located in telomeric regions. Although the residence time estimates of these four peaks are probably accurate, we noticed that other characteristics were very distinct from other peaks (*e.g.* nucleosome organisation, motif composition, RNA polymerase II binding). Therefore, these peaks were excluded, yielding a total of 191 Abf1-binding sites that were analysed in greater detail.

Exponential decay fitting

To fit the exponential decay model, first the bam files were centred and smoothed with a 101bp window, as described in (de Jonge *et al*, 2017). Subsequently, all samples were scaled to 1 million reads using genomecov from the bedtools2 suite v2.27 (Quinlan & Hall, 2010), which makes sure that total coverage across the genome is the same for all samples (1.01 x 10^8 bases). For each binding site (*n*=191) the total coverage was calculated for each sample in a window ± 50 bp from the peak summit. These values were used to fit a first-order exponential decay function using the `nls` function in R:

$$y(t) = y_f + (y_0 - y_f)e^{-k_{off}t} \qquad (1)$$

with y_0 the binding levels a *t*=0 (*i.e.* before depletion), *t* the time since depletion, y_f the final binding level and k_{off} the decay rate of the binding levels. The residence time is given by $1/k_{off}$ and represents the average time Abf1 stays bound to a specific site. The fits were done in R with the `nls` function using the formula: "`nls(ChIP ~ SSasymp(time, yf, y0, log_koff), data = data)`", yielding regressions with excellent R^2, with the lowest R^2 = 0.63 and the median R^2 = 0.95 (**Supplemental Fig S2C**). One of the 10 minute depletion ChIP samples had much higher binding levels compared to the other 10 minutes samples, with a median absolute deviation more than six times as high. Upon removal of this sample all fits improved. This sample was therefore removed from all analyses. The 191 binding sties were divided into four residence time groups defined by the quartiles of their residence times (48 or 47 sites per quartile).

4tU-seq expression analysis

The 4tU-seq reads were assigned to genomic features using featureCounts from the subread package v1.6.5 (Liao *et al*, 2014). As an annotation file, transcription start site annotations from (van Bakel *et al*, 2013) were merged with the genome annotation from the Saccharomyces genome database (SGD) (Cherry *et al*, 2012) containing ORFs, tRNAs, rRNAs and snRNAs. The counts from the two independent sequence runs were combined and differential expression of the genomic features (genes) was calculated using the DESeq2 package v1.10.1 (Love *et al*, 2014) in R. Only genes with a fold change of more than 1.5 with an adjusted *p*-value < 0.01 after 20 minutes as well as 30 minutes of depletion were considered differentially expressed. The fold change in mRNA synthesis was calculated relative to *t*=0.

To model the decrease rate of mRNA synthesis, absolute transcript counts were used at each time point. They were normalized to the median number of transcripts of all samples after filtering out rRNAs. Only genes that were significantly downregulated with Abf1 binding to the promoter were used (*n*=88). Binding peaks were assigned to genes when the summit of that peak was found within the promoter (500 bp upstream of the transcription start site). As described for the ChIP-seq data, a first-order exponential decay function (Eq. 1) was used to model the changes in mRNA synthesis. In this case y_0 is the expression level before depletion and k_{off} is the rate with which the expression decreases to the final expression level y_f. For six of the genes with robust changes in mRNA synthesis no reliable fit could

be obtained and these were therefore excluded from **Fig 2G** (*n*=82).

External datasets

To assess what percentage of Abf1 binding peaks overlap with previously detected Abf1 binding sites, the peaks (peak summits ± 50 bp) detected here (*n*=948) were compared to published data sets. Data from three different techniques were used: ORGANIC, ChEC-seq and ChIP-exo (Kasinathan *et al*, 2014; Zentner *et al*, 2015; Rossi *et al*, 2018b). For the ORGANIC data the published bound Abf1 sites (*n*=1068) from the "10′ MNase 80mM" samples were used (Kasinathan *et al*, 2014). For the ChEC-seq data the Abf1 sites that were both classified as "fast" and "high scoring motif" (*n*=1583) were taken (Zentner *et al*, 2015). For the ChIP-exo peaks, all sites detected using the ChIP-exo protocol v5 (*n*=3177) were used (Rossi *et al*, 2018b).

To assess *in vivo* protection from MNase cleavage, the bigwig files "Abf1aa_V_freeMNase_ChEC" and "Abf1aa_R_freeMNase_ChEC" were downloaded from the gene expression omnibus (GEO) dataset GSE98259 (Kubik *et al*, 2018) and smoothed with a 3 bp window. The data were centred on the Abf1 binding motif and the average number of cleavage sites per residence time quartile were calculated. Subsequently, the average number of cut sites was calculated in the area of the motif (-8 bp to +8 bp from the motif midpoint) both in the presence and absence of Abf1. The cleavage ratio was calculated by taking the number of cuts in the absence of Abf1 divided by the number of cuts in the presence of Abf1. Sites without cuts in either conditions (with or without rapamycin) were excluded from the quantification (**Fig 1J**).

To compare synthesis rates with off-rates, residence times and binding levels, genome-wide synthesis rates were taken from (Sun *et al*, 2012), by downloading them from the researchers' website: https://www.mpibpc.mpg.de/13760807/Sc_turnover.zip.

To visualize nucleosome positioning before and after depletion of Abf1, the bigwig files "Abf1veh15" and "Abf1rapa15" were downloaded from GEO dataset GSE73337 (Kubik *et al*, 2015). The data were either centred on the Abf1 binding motif (**Fig 2**) or aligned on the +1 nucleosome (**Fig 3B**), with +1 nucleosome positions taken from (Kubik *et al*, 2015). The average nucleosome occupancy was calculated for genes with Abf1 binding, an annotated +1 nucleosome and that were strongly downregulated (fold change > 2 at *t*=20, *n*=44), weakly downregulated (1.5 < fold change < 2 at *t*=20, *n*=42) or did not change (fold change < 1.5 at *t*=20, *n*=112) upon depletion of Abf1 (**Fig 3B**). In **Fig 2** the average nucleosome occupancy was calculated per residence time quartile.

To visualize polymerase binding, the PAR-CLIP (photoactivatable ribonucleoside-enhanced cross-linking and immunoprecipitation) data for both the plus and minus strand from sample "Rpb2-HTB Control With Rapamycin" were downloaded from GEO dataset GSE56435 (Schaughency *et al*, 2014). As the Abf1 motif is strand-specific, the data were reoriented accordingly, meaning that when the data had to be reoriented to match the orientation of the motif (as shown in **Fig 5C**), the plus and minus strand were also swapped. To calculate the roadblock efficiency, the average binding in the roadblocked peak, located at -37 bp ± 5 bp from the Abf1 binding motif centre, was normalized by the amount of incoming transcription (defined as the average Pol II binding in the region from -300 bp until -100 bp upstream of the Abf1 binding motif). For the quantification shown in **Fig 4C,** a peak was considered to be a roadblock peak when it had upstream normalized Pol II binding > 2. With this cut-off approximately 25% of the peaks (49/191) were considered to be a roadblock for Pol II.

Motif scoring and DNA shape analysis

The position frequency matrix from (MacIsaac *et al*, 2006) was obtained from the YeTFaSCo database (Boer & Hughes, 2011), multiplied by a factor 1000 and converted to a position weight matrix (PWM). The region ± 100 bp of the summit of each binding peak was searched for a match of this PWM using the matchPWM function from the Biostrings v2.38.4 package in R, using a minimum motif score of 85%. Whenever a binding peak had more than one motif match, the highest score was assigned to this binding peak. For all aggregate plots, the data was aligned to the motif with the highest motif score with all motifs in the same orientation as shown in **Fig 5C**. DNA shape analysis was done on the aligned motifs ± 40 bp from the motif midpoint using DNAshapeR v1.10.0 (Chiu *et al*, 2016). The DNA shape of the bound and unbound sites from (Rossi *et al*, 2018a) was calculated as described in (Rossi *et al*, 2018a), by taking for each of the 8 motifs the top 50 and bottom 50 bound peaks and showing the average of the top 400 and bottom 400 bound peaks. For further details see (Rossi *et al*, 2018a).

Statistical analysis and data visualisation

All statistical analyses were done using the statistical language R v3.2.2 except for the DNA shape and Venn diagram analyses which were done using R v3.5.1. The area-proportional Venn diagrams were created using the eulerr package v6.0.0 in R v3.5.1.

To visualize the binding to different genomic loci in **Fig 1B**, the Sushi package v1.24.0 was used (Phanstiel *et al*, 2014). All boxplots were created using R's built-in `boxplot` function, with default settings; here the solid horizontal line represent the median, the box shows the interquartile range and the whiskers are at the most extreme data point no further away from the closest quartile than 1.5 times the interquartile range. Differences between the four residence time quartiles

were assessed using a one-way ANOVA followed by Tukey's honest significant difference test (**Fig 1J, 4B, 5B** and **5D**). The difference between the two groups in **Fig 4C** was tested using a two-tailed t-test and between the groups in **Fig 5A** using a Wilcoxon rank-sum test, since one of the groups was deemed to deviate too much from normality.

Acknowledgements

We thank the members of the Holstege and Kemmeren groups for their support and discussions. We thank Jeff DeMartino and Marit de Kort for technical assistance. This work was supported by the Netherlands Organisation for Scientific Research (NWO) grant 86411010 and by the European Research Council (ERC) grant 671174 DynaMech.

References

Adams CC, Workman JL (1995) Binding of disparate transcriptional activators to nucleosomal DNA is inherently cooperative. *Mol Cell Biol* 15: 1405–1421

van Bakel H, Tsui K, Gebbia M, Mnaimneh S, Hughes TR, Nislow C (2013) A compendium of nucleosome and transcript profiles reveals determinants of chromatin architecture and transcription. *PLoS Genet* 9: e1003479

Bayle JH, Grimley JS, Stankunas K, Gestwicki JE, Wandless TJ, Crabtree GR (2006) Rapamycin Analogs with Differential Binding Specificity Permit Orthogonal Control of Protein Activity. *Chem Biol* 13: 99–107

Boer CG de, Hughes TR (2011) YeTFaSCo: a database of evaluated yeast transcription factor sequence specificities. *Nucleic Acids Res*: gkr993

Bosisio D, Marazzi I, Agresti A, Shimizu N, Bianchi ME, Natoli G (2006) A hyper-dynamic equilibrium between promoter-bound and nucleoplasmic dimers controls NF-κB-dependent gene activity. *EMBO J* 25: 798–810

Brahma S, Henikoff S (2020) Epigenome Regulation by Dynamic Nucleosome Unwrapping. *Trends Biochem Sci* 45: 13–26

Brignall R, Moody AT, Mathew S, Gaudet S (2019) Considering Abundance, Affinity, and Binding Site Availability in the NF-κB Target Selection Puzzle. *Front Immunol* 10: 609

Buchman AR, Kornberg RD (1990) A yeast ARS-binding protein activates transcription synergistically in combination with other weak activating factors. *Mol Cell Biol* 10: 887–897

Busch A, Kiel T, Hübner S (2009) Quantification of Nuclear Protein Transport using Induced Heterodimerization. *Traffic* 10: 1221–1227

Candelli T, Challal D, Briand J-B, Boulay J, Porrua O, Colin J, Libri D (2018) High-resolution transcription maps reveal the widespread impact of roadblock termination in yeast. *EMBO J* 37: e97490

Cherry JM, Hong EL, Amundsen C, Balakrishnan R, Binkley G, Chan ET, Christie KR, Costanzo MC, Dwight SS, Engel SR, Fisk DG, Hirschman JE, Hitz BC, Karra K, Krieger CJ, Miyasato SR, Nash RS, Park J, Skrzypek MS, Simison M, *et al* (2012) Saccharomyces Genome Database: the genomics resource of budding yeast. *Nucleic Acids Res* 40: D700-705

Chiu T-P, Comoglio F, Zhou T, Yang L, Paro R, Rohs R (2016) DNAshapeR: an R/Bioconductor package for DNA shape prediction and feature encoding. *Bioinformatics* 32: 1211–1213

Coleman RA, Liu Z, Darzacq X, Tjian R, Singer RH, Lionnet T (2015) Imaging Transcription: Past, Present, and Future. *Cold Spring Harb Symp Quant Biol* 80: 1–8

Colin J, Candelli T, Porrua O, Boulay J, Zhu C, Lacroute F, Steinmetz LM, Libri D (2014) Roadblock Termination by Reb1p Restricts Cryptic and Readthrough Transcription. *Mol Cell* 56: 667–680

Collas P (2010) The current state of chromatin immunoprecipitation. *Mol Biotechnol* 45: 87–100

Cramer P (2019) Organization and regulation of gene transcription. *Nature* 573: 45–54

Dion MF, Kaplan T, Kim M, Buratowski S, Friedman N, Rando OJ (2007) Dynamics of replication-independent histone turnover in budding yeast. *Science* 315: 1405–1408

Dölken L, Ruzsics Z, Rädle B, Friedel CC, Zimmer R, Mages J, Hoffmann R, Dickinson P, Forster T, Ghazal P, Koszinowski UH (2008) High-resolution gene expression profiling for simultaneous kinetic parameter analysis of RNA synthesis and decay. *RNA* 14: 1959–1972

Donovan BT, Chen H, Jipa C, Bai L, Poirier MG (2019a) Dissociation rate compensation mechanism for budding yeast pioneer transcription factors. *eLife* 8: e43008

Donovan BT, Huynh A, Ball DA, Patel HP, Poirier MG, Larson DR, Ferguson ML, Lenstra TL (2019b) Live-cell imaging reveals the interplay between transcription factors, nucleosomes, and bursting. *EMBO J* 38: e100809

Elbi C, Walker DA, Romero G, Sullivan WP, Toft DO, Hager GL, DeFranco DB (2004) Molecular chaperones function as steroid receptor nuclear mobility factors. *Proc Natl Acad Sci* 101: 2876–2881

Elf J, Barkefors I (2019) Single-Molecule Kinetics in Living Cells. *Annu Rev Biochem* 88: 635–659

Enomoto S, Longtine MS, Berman J (1994) Enhancement of Telomere-Plasmid Segregation by the X-Telomere Associated Sequence in Saccharomyces Cerevisiae Involves Sir2, Sir3, Sir4 and Abf1. *Genetics* 136: 757–767

Friedman N, Rando OJ (2015) Epigenomics and the structure of the living genome. *Genome Res* 25: 1482–1490

Furey TS (2012) ChIP–seq and beyond: new and improved methodologies to detect and characterize protein–DNA interactions. *Nat Rev Genet* 13: 840–852

Gailus-Durner V, Xie J, Chintamaneni C, Vershon AK (1996) Participation of the yeast activator Abf1 in meiosis-specific expression of the HOP1 gene. *Mol Cell Biol* 16: 2777–2786

Ganapathi M, Palumbo MJ, Ansari SA, He Q, Tsui K, Nislow C, Morse RH (2011) Extensive role of the general regulatory factors, Abf1 and Rap1, in determining genome-wide chromatin structure in budding yeast. *Nucleic Acids Res* 39: 2032–2044

Garbett KA, Tripathi MK, Cencki B, Layer JH, Weil PA (2007) Yeast TFIID Serves as a Coactivator for Rap1p by Direct Protein-Protein Interaction. *Mol Cell Biol* 27: 297–311

Gilmour DS, Lis JT (1984) Detecting protein-DNA interactions in vivo: distribution of RNA polymerase on specific bacterial genes. *Proc Natl Acad Sci U S A* 81: 4275–4279

Grimaldi Y, Ferrari P, Strubin M (2014) Independent RNA polymerase II preinitiation complex dynamics and nucleosome turnover at promoter sites in vivo. *Genome Res* 24: 117–124

Hager GL, McNally JG, Misteli T (2009) Transcription dynamics. *Mol Cell* 35: 741–753

Hahn S, Young ET (2011) Transcriptional regulation in Saccharomyces cerevisiae: transcription factor regulation

and function, mechanisms of initiation, and roles of activators and coactivators. *Genetics* 189: 705–736

Halfter H, Kavety B, Vandekerckhove J, Kiefer F, Gallwitz D (1989) Sequence, expression and mutational analysis of BAF1, a transcriptional activator and ARS1-binding protein of the yeast Saccharomyces cerevisiae. *EMBO J* 8: 4265–4272

Hammar P, Walldén M, Fange D, Persson F, Baltekin O, Ullman G, Leroy P, Elf J (2014) Direct measurement of transcription factor dissociation excludes a simple operator occupancy model for gene regulation. *Nat Genet* 46: 405–408

Hartley PD, Madhani HD (2009) Mechanisms that specify promoter nucleosome location and identity. *Cell* 137: 445–458

Haruki H, Nishikawa J, Laemmli UK (2008) The anchor-away technique: rapid, conditional establishment of yeast mutant phenotypes. *Mol Cell* 31: 925–932

Hasegawa Y, Struhl K (2019) Promoter-specific dynamics of TATA-binding protein association with the human genome. *Genome Res* 29: 1939–1950

Ho B, Baryshnikova A, Brown GW (2018) Unification of Protein Abundance Datasets Yields a Quantitative Saccharomyces cerevisiae Proteome. *Cell Syst* 6: 192-205.e3

Hoopes BC, LeBlanc JF, Hawley DK (1992) Kinetic analysis of yeast TFIID-TATA box complex formation suggests a multi-step pathway. *J Biol Chem* 267: 11539–11547

de Jonge WJ, Brok M, Kemmeren P, Holstege FCP (2019) An extensively optimized chromatin immunoprecipitation protocol for quantitatively comparable and robust results. *bioRxiv*: 835926

de Jonge WJ, Brok M, Kemmeren P, Holstege FCP (2020) An Optimized Chromatin Immunoprecipitation Protocol for Quantification of Protein-DNA Interactions. *STAR Protoc* Available at: https://star-protocols.cell.com/protocols/71

de Jonge WJ, O'Duibhir E, Lijnzaad P, van Leenen D, Groot Koerkamp MJ, Kemmeren P, Holstege FC (2017) Molecular mechanisms that distinguish TFIID housekeeping from regulatable SAGA promoters. *EMBO J* 36: 274–290

Karpova TS, Chen TY, Sprague BL, McNally JG (2004) Dynamic interactions of a transcription factor with DNA are accelerated by a chromatin remodeller. *EMBO Rep* 5: 1064–1070

Karpova TS, Kim MJ, Spriet C, Nalley K, Stasevich TJ, Kherrouche Z, Heliot L, McNally JG (2008) Concurrent Fast and Slow Cycling of a Transcriptional Activator at an Endogenous Promoter. *Science* 319: 466–469

Kasinathan S, Orsi GA, Zentner GE, Ahmad K, Henikoff S (2014) High-resolution mapping of transcription factor binding sites on native chromatin. *Nat Methods* 11: 203–209

Kim D, Langmead B, Salzberg SL (2015) HISAT: a fast spliced aligner with low memory requirements. *Nat Methods* 12: 357–360

Kivioja T, Vähärautio A, Karlsson K, Bonke M, Enge M, Linnarsson S, Taipale J (2012) Counting absolute numbers of molecules using unique molecular identifiers. *Nat Methods* 9: 72–74

Klemm JD, Beals CR, Crabtree GR (1997) Rapid targeting of nuclear proteins to the cytoplasm. *Curr Biol* 7: 638–644

Kloster-Landsberg M, Herbomel G, Wang I, Derouard J, Vourc'h C, Usson Y, Souchier C, Delon A (2012) Cellular response to heat shock studied by multiconfocal fluorescence correlation spectroscopy. *Biophys J* 103: 1110–1119

Krietenstein N, Wal M, Watanabe S, Park B, Peterson CL, Pugh BF, Korber P (2016) Genomic Nucleosome Organization Reconstituted with Pure Proteins. *Cell* 167: 709-721.e12

Kubik S, Bruzzone MJ, Jacquet P, Falcone J-L, Rougemont J, Shore D (2015) Nucleosome Stability Distinguishes Two Different Promoter Types at All Protein-Coding Genes in Yeast. *Mol Cell* 60: 422–434

Kubik S, Bruzzone MJ, Shore D (2017) Establishing nucleosome architecture and stability at promoters: Roles of pioneer transcription factors and the RSC chromatin remodeler. *BioEssays* 39: 1600237

Kubik S, O'Duibhir E, de Jonge WJ, Mattarocci S, Albert B, Falcone J-L, Bruzzone MJ, Holstege FCP, Shore D (2018) Sequence-Directed Action of RSC Remodeler and General Regulatory Factors Modulates +1 Nucleosome Position to Facilitate Transcription. *Mol Cell* 71: 89-102.e5

Kuo MH, Allis CD (1999) In vivo cross-linking and immunoprecipitation for studying dynamic Protein:DNA associations in a chromatin environment. *Methods San Diego Calif* 19: 425–433

de Laat W, Dekker J (2012) 3C-based technologies to study the shape of the genome. *Methods* 58: 189–191

Lai WKM, Pugh BF (2017) Understanding nucleosome dynamics and their links to gene expression and DNA replication. *Nat Rev Mol Cell Biol* 18: 548–562

Larson DR (2011) What do expression dynamics tell us about the mechanism of transcription? *Curr Opin Genet Dev* 21: 591–599

Lascaris RF, Groot E de, Hoen P-B, Mager WH, Planta RJ (2000) Different roles for Abf1p and a T-rich promoter element in nucleosome organization of the yeast RPS28A gene. *Nucleic Acids Res* 28: 1390–1396

Levo M, Avnit-Sagi T, Lotan-Pompan M, Kalma Y, Weinberger A, Yakhini Z, Segal E (2017) Systematic Investigation of Transcription Factor Activity in the Context of Chromatin Using Massively Parallel Binding and Expression Assays. *Mol Cell* 65: 604-617.e6

Liao Y, Smyth GK, Shi W (2014) featureCounts: an efficient general purpose program for assigning sequence reads to genomic features. *Bioinforma Oxf Engl* 30: 923–930

Lickwar CR, Mueller F, Hanlon SE, McNally JG, Lieb JD (2012) Genome-wide protein–DNA binding dynamics suggest a molecular clutch for transcription factor function. *Nature* 484: 251–255

Love MI, Huber W, Anders S (2014) Moderated estimation of fold change and dispersion for RNA-seq data with DESeq2. *Genome Biol* 15: 550

Luo Y, North JA, Rose SD, Poirier MG (2014) Nucleosomes accelerate transcription factor dissociation. *Nucleic Acids Res* 42: 3017–3027

MacIsaac KD, Wang T, Gordon DB, Gifford DK, Stormo GD, Fraenkel E (2006) An improved map of conserved regulatory sites for Saccharomyces cerevisiae. *BMC Bioinformatics* 7: 113

Marahrens Y, Stillman B (1992) A yeast chromosomal origin of DNA replication defined by multiple functional elements. *Science* 255: 817–823

McNally JG, Müller WG, Walker D, Wolford R, Hager GL (2000) The Glucocorticoid Receptor: Rapid Exchange with Regulatory Sites in Living Cells. *Science* 287: 1262–1265

Miller JA, Widom J (2003) Collaborative Competition Mechanism for Gene Activation In Vivo. *Mol Cell Biol* 23: 1623–1632

Mirny LA (2010) Nucleosome-mediated cooperativity between transcription factors. *Proc Natl Acad Sci* 107: 22534–22539

Mivelaz M, Cao A-M, Kubik S, Zencir S, Hovius R, Boichenko I, Stachowicz AM, Kurat CF, Shore D, Fierz B (2020) Chromatin Fiber Invasion and Nucleosome Displacement by the Rap1 Transcription Factor. *Mol Cell* 77: 488-500.e9

Miyake T, Loch CM, Li R (2002) Identification of a Multifunctional Domain in Autonomously Replicating Sequence-Binding Factor 1 Required for Transcriptional Activation, DNA Replication, and Gene Silencing. *Mol Cell Biol* 22: 505–516

Miyake T, Reese J, Loch CM, Auble DT, Li R (2004) Genome-wide analysis of ARS (autonomously replicating sequence) binding factor 1 (Abf1p)-mediated transcriptional regulation in Saccharomyces cerevisiae. *J Biol Chem* 279: 34865–34872

Mueller F, Stasevich TJ, Mazza D, McNally JG (2013) Quantifying transcription factor kinetics: At work or at play? *Crit Rev Biochem Mol Biol* 48: 492–514

Park D, Lee Y, Bhupindersingh G, Iyer VR (2013) Widespread misinterpretable ChIP-seq bias in yeast. *PloS One* 8: e83506

Park PJ (2009) ChIP–seq: advantages and challenges of a maturing technology. *Nat Rev Genet* 10: 669–680

Paul E, Tirosh I, Lai W, Buck MJ, Palumbo MJ, Morse RH (2015) Chromatin Mediation of a Transcriptional Memory Effect in Yeast. *G3 Genes Genomes Genet* 5: 829–838

Perlmann T, Eriksson P, Wrange O (1990) Quantitative analysis of the glucocorticoid receptor-DNA interaction at the mouse mammary tumor virus glucocorticoid response element. *J Biol Chem* 265: 17222–17229

Phanstiel DH, Boyle AP, Araya CL, Snyder MP (2014) Sushi.R: flexible, quantitative and integrative genomic visualizations for publication-quality multi-panel figures. *Bioinformatics* 30: 2808–2810

Polach KJ, Widom J (1996) A Model for the Cooperative Binding of Eukaryotic Regulatory Proteins to Nucleosomal Target Sites. *J Mol Biol* 258: 800–812

Poorey K, Viswanathan R, Carver MN, Karpova TS, Cirimotich SM, McNally JG, Bekiranov S, Auble DT (2013) Measuring Chromatin Interaction Dynamics on the Second Time Scale at Single-Copy Genes. *Science* 342: 369–372

Pryde FE, Louis EJ (1999) Limitations of silencing at native yeast telomeres. *EMBO J* 18: 2538–2550

Quinlan AR, Hall IM (2010) BEDTools: a flexible suite of utilities for comparing genomic features. *Bioinforma Oxf Engl* 26: 841–842

Reed SH, Akiyama M, Stillman B, Friedberg EC (1999) Yeast autonomously replicating sequence binding factor is involved in nucleotide excision repair. *Genes Dev* 13: 3052–3058

Rhode PR, Sweder KS, Oegema KF, Campbell JL (1989) The gene encoding ARS-binding factor I is essential for the viability of yeast. *Genes Dev* 3: 1926–1939

Rossi MJ, Lai WKM, Pugh BF (2018a) Genome-wide determinants of sequence-specific DNA binding of general regulatory factors. *Genome Res* 28: 497–508

Rossi MJ, Lai WKM, Pugh BF (2018b) Simplified ChIP-exo assays. *Nat Commun* 9: 1–13

Roy K, Chanfreau GF (2018) A global function for transcription factors in assisting RNA polymerase II termination. *Transcription* 9: 41–46

Roy K, Gabunilas J, Gillespie A, Ngo D, Chanfreau GF (2016) Common genomic elements promote transcriptional and DNA replication roadblocks. *Genome Res* 26: 1363–1375

Rufiange A, Jacques P-É, Bhat W, Robert F, Nourani A (2007) Genome-Wide Replication-Independent Histone H3 Exchange Occurs Predominantly at Promoters and Implicates H3 K56 Acetylation and Asf1. *Mol Cell* 27: 393–405

Schaughency P, Merran J, Corden JL (2014) Genome-wide mapping of yeast RNA polymerase II termination. *PLoS Genet* 10: e1004632

Schermer UJ, Korber P, Hörz W (2005) Histones Are Incorporated in trans during Reassembly of the Yeast PHO5 Promoter. *Mol Cell* 19: 279–285

Schroeder SC, Weil PA (1998) Genetic Tests of the Role of Abf1p in Driving Transcription of the Yeast TATA Box Bindng Protein-encoding Gene,SPT15. *J Biol Chem* 273: 19884–19891

Skene PJ, Henikoff S (2017) An efficient targeted nuclease strategy for high-resolution mapping of DNA binding sites. *eLife* 6: e21856

Southern JA, Young DF, Heaney F, Baumgärtner WK, Randall RE (1991) Identification of an epitope on the P and V proteins of simian virus 5 that distinguishes between two isolates with different biological characteristics. *J Gen Virol* 72: 1551–1557

Spitz F, Furlong EEM (2012) Transcription factors: from enhancer binding to developmental control. *Nat Rev Genet* 13: 613–626

Stavreva DA, Müller WG, Hager GL, Smith CL, McNally JG (2004) Rapid glucocorticoid receptor exchange at a promoter is coupled to transcription and regulated by chaperones and proteasomes. *Mol Cell Biol* 24: 2682–2697

Struhl K, Segal E (2013) Determinants of nucleosome positioning. *Nat Struct Mol Biol* 20: 267–273

Sun M, Schwalb B, Schulz D, Pirkl N, Etzold S, Larivière L, Maier KC, Seizl M, Tresch A, Cramer P (2012) Comparative dynamic transcriptome analysis (cDTA) reveals mutual feedback between mRNA synthesis and degradation. *Genome Res* 22: 1350–1359

Teytelman L, Thurtle DM, Rine J, van Oudenaarden A (2013) Highly expressed loci are vulnerable to misleading ChIP localization of multiple unrelated proteins. *Proc Natl Acad Sci U S A* 110: 18602–18607

Venditti P, Costanzo G, Negri R, Camilloni G (1994) ABFI contributes to the chromatin organization of Saccharomyces cerevisiae ARS1 B-domain. *Biochim Biophys Acta BBA - Gene Struct Expr* 1219: 677–689

Voss TC, Hager GL (2014) Dynamic regulation of transcriptional states by chromatin and transcription factors. *Nat Rev Genet* 15: 69–81

Warner JR (1999) The economics of ribosome biosynthesis in yeast. *Trends Biochem Sci* 24: 437–440

van Werven FJ, van Teeffelen HAAM, Holstege FCP, Timmers HTM (2009) Distinct promoter dynamics of the basal transcription factor TBP across the yeast genome. *Nat Struct Mol Biol* 16: 1043–1048

Woo H, Ha SD, Lee SB, Buratowski S, Kim T (2017) Modulation of gene expression dynamics by co-transcriptional histone methylations. *Exp Mol Med* 49: e326–e326

Yao J, Munson KM, Webb WW, Lis JT (2006) Dynamics of heat shock factor association with native gene loci in living cells. *Nature* 442: 1050–1053

Yarragudi A, Miyake T, Li R, Morse RH (2004) Comparison of ABF1 and RAP1 in chromatin opening and transactivator potentiation in the budding yeast Saccharomyces cerevisiae. *Mol Cell Biol* 24: 9152–9164

Yarragudi A, Parfrey LW, Morse RH (2007) Genome-wide analysis of transcriptional dependence and probable target sites for Abf1 and Rap1 in Saccharomyces cerevisiae. *Nucleic Acids Res* 35: 193–202

Zaidi H, Hoffman EA, Shetty SJ, Bekiranov S, Auble DT (2017) Second-generation method for analysis of chromatin binding with formaldehyde–cross-linking kinetics. *J Biol Chem* 292: 19338–19355

Zaret KS, Carroll JS (2011) Pioneer transcription factors:

establishing competence for gene expression. *Genes Dev* 25: 2227–2241

Zentner GE, Kasinathan S, Xin B, Rohs R, Henikoff S (2015) ChEC-seq kinetics discriminates transcription factor binding sites by DNA sequence and shape in vivo. *Nat Commun* 6: 8733

Zhang Y, Liu T, Meyer CA, Eeckhoute J, Johnson DS, Bernstein BE, Nusbaum C, Myers RM, Brown M, Li W, Liu XS (2008) Model-based analysis of ChIP-Seq (MACS). *Genome Biol* 9: R137